



Performance Evaluation of CNTFETs Fabricated with Carbon Nanotubes of Different Synthesis Methods

Iskandar Yahya^{1*}, Muhammad Azuddin Hassan², Seri Mastura Mustaza¹, Huda Abdullah¹, Steven K. Clowes³, S. Ravi. P. Silva³

¹Department of Electrical, Electronic & Systems Engineering,
Universiti Kebangsaan Malaysia, Bangi Selangor, 43600, MALAYSIA.

²Institute of Microengineering & Nanoelectronics (IMEN),
Universiti Kebangsaan Malaysia, Bangi Selangor, 43600, MALAYSIA.

³Advanced Technology Institute,
University of Surrey Guildford, Surrey, GU2 7XH, UNITED KINGDOM.

*Corresponding Author

DOI: <https://doi.org/10.30880/ijie.2022.14.03.022>

Received 30 November 2021; Accepted 07 June 2022; Available online 20 June 2022

Abstract: Single walled carbon nanotubes (SWCNTs) exhibit extraordinary electronic properties that render it as an exciting candidate to be applied as the active channel of high-performance carbon nanotube field effect transistors (CNTFETs). The electronic properties of SWCNTs have been demonstrated to be dependent on the tube intrinsic properties that includes structural defects, chirality and diameter. Structural tube defects can be affected by the synthesis method and therefore the latter should also affect the device performance. Hence, this paper aims to present the influence of SWCNTs source synthesis method towards the resulting CNTFET device characteristics. A total of four SWCNT samples were sourced from different synthesis methods in fabricating CNTFETs. The synthesis methods are arc-discharge and three different variation of chemical vapor deposition (CVD) processes, which are DIPS, HiPco and CoMoCAT, respectively. Prior to fabrication, the SWCNT samples were characterized via Raman spectroscopy to quantify the tube defect levels of each sample, which are directly proportional to the G -peak to D -peak height ratio, G/D . Electrical characterization was carried out via 3-terminal field effect I - V measurement to evaluate key device performance parameters such as on-off current ratio, I_{ON}/I_{OFF} , transconductance, g_m , subthreshold slope, S_p and field effect mobility, μ_{FE} . Analysis shows that G/D affects the I_{OFF} more significantly relative to I_{ON} , resulting in increasing I_{ON}/I_{OFF} , and hence switching performance, when G/D increases. It is shown an increase of $\sim 50\%$ to the G/D of the SWCNT source resulted in $\sim 860\%$ increase in μ_{FE} . Based on the correlation between the optical analysis and electrical measurement, we conclude that the SWCNT growth method can significantly affect the CNTFET device performance.

Keywords: Single walled carbon nanotube, field effect transistor, defect

1. Introduction

Single walled carbon nanotubes (SWCNTs) exhibit exceptional electronic properties including high carrier mobility, structural robustness and can display either semiconducting or metallic electronic type, making it a promising 1D material for advance electronic device applications [1]. One particular application is carbon nanotube field effect transistor (CNTFET) whereby semiconducting SWCNTs (s-SWCNTs) are applied as the active channel of a high-performance

*Corresponding author: iskandar.yahya@ukm.edu.my

field effect transistor (FET). High performance CNTFETs should display precise source-drain current modulation that requires the active channel to consist of entirely s-SWCNTs. Obtaining exclusively s-SWCNTs is not straightforward since generally and statistically, the conventional synthesis of SWCNTs yields heterogenous s-SWCNTs and metallic (m-SWCNTs) mixture at a ratio of 2:1, respectively [2], [3]. For the SWCNTs to be used in fabricating CNTFETs, the as synthesized SWCNT source must be separated based on electronic type to obtain high purity s-SWCNTs with little to no traces of m-SWCNTs.

Realizing large scale application of CNTFETs in the form of integrated circuits require reproducible and consistent individual device performance. The latter can be affected by the structural properties of the SWCNTs applied in the active channel such as the tube diameter [4], [5]. Variation to the structural and electronic properties of SWCNTs may exist between samples synthesized via different processes such as tube diameter distribution, band gap and the level of structural defects, which can be observed from optical characterizations [6]. By using resonance Raman spectroscopy (RRS) for example, variation to such tube properties can be observed. Therefore, it is imperative to conduct a study of the influence of SWCNT synthesis process towards the device performance of the resulting CNTFETs.

In this paper, we present our work on the analysis of the effect of SWCNT source synthesis process towards the fabricated CNTFET's device performance. Here, SWCNT sources from four different synthesis processes were applied as the source to drain channel of a substrate backgated CNTFET. Prior to the device fabrication, the SWCNT samples were subjected to optical characterization via RSS to evaluate the level of tube defect. After CNTFET fabrication, electrical characterization was done. By correlating device characteristics to the measured optical characterization, we were able to demonstrate the effect of SWCNT synthesis process towards the fabricated CNTFETs' device performance.

2. Methodology

The methodology of this work is divided into four distinct phases, which are the SWCNT source preparation, optical characterization via resonance Raman spectroscopy (RRS), CNTFET device fabrication process and electrical characterization. The following describes briefly each phase, respectively.

2.1 SWCNT Source and Preparation

In this study, four SWCNT samples, each synthesized using different method, were directly sourced from the respective manufacturers. The details of each SWCNT sample are shown in Table 1, which are identified as DIPS, ADCNT, HiPco, and CoMoCAT. The labelling of the SWCNT samples were chosen to reflect the synthesis process of each respective source. Other than being some of the most established synthesis processes of commercially available SWCNT sources, the samples were chosen due to the comprehensive coverage of tube diameter distribution, and hence tube chirality. Sample DIPS are chemical vapor deposition (CVD) synthesized SWCNTs via direct injection pyrolytic synthesis (DIPS) route and have tube diameter range of 0.8 – 3.0 nm [7]. Sample ADCNT are arc-discharged synthesized SWCNTs with tube diameter distribution of 1.2 – 1.4 nm. Sample HiPco are CVD synthesized SWCNTs via high pressure carbon monoxide and display relatively narrow tube diameter distribution of 0.8 – 1.0 nm [8]. Sample CoMoCAT are CVD synthesized SWCNTs via process similar to that of HiPco but using cobalt (Co) and molybdenum oxide (MoO₃) catalysts. Sample CoMoCAT display the smallest average tube diameter ranging from 0.7 to 0.9 nm [9].

All of the SWCNTs samples were in the form of powdered solids, except for sample DIPS that was in the form of buckypaper. The SWCNT samples were dispersed in deionized water at 1mg/10ml weight to volume (wt./v) ratio mixed with 2% sodium dodecyl sulphate (SDS, *Sigma-Aldrich*) forming an aqueous solution. The SDS were to added to act as surfactant to promote debundling of SWCNTs into single isolated suspended tubes in the solution. The samples were then subjected to ultrasonic tip probe agitation at for 4 hours active time using 40% of 750 kW power at 20 kHz to initiate the peeling of SWCNT bundles into single isolated tubes.

Table 1 – Sources of SWCNT used

Sample Name	Properties		
	Synthesis Method	Diameter Distribution	Source
DIPS	CVD via DIPS	0.8 – 3 nm	Nikkiso, Japan
ADCNT	Arc Discharge	1.2 – 1.4 nm	Nanocarblab
HiPco	CVD via High pressure carbon monoxide	0.8 – 1.0 nm	Nanointegris
CoMoCAT	CVD via Cobalt & Molybdenum oxide catalysts.	0.7 – 0.9 nm	Sigma-Aldrich

After ultrasonication, the remaining SWCNT bundles were segregated from the isolated tubes via centrifugation at 200K times gravity for 20 minutes. The supernatants of the centrifuge step were collected for the next step, which is the SWCNT electronic type separation.

The electronic type separation SWCNTs were done via gel agarose column chromatography (GACC) process, originally proposed by Tanaka et. al [10], to obtain m-SWCNT and s-SWCNT enriched samples, which the latter were used to fabricate CNTFETs in this study. The detailed description and characterization of the separation process of SWCNT samples used in this study have been published elsewhere previously [11]. Here, only brief explanation of the method and mechanism is provided. A continuous separation syringe column was filled with 1.5 ml of agarose microbeads suspended in ethanol (Sephacrose 2B, 60 – 200 μm , Sigma-Aldrich) and washed by pipetting 5 ml of SDS solution from the top to disperse the ethanol. The separation process was initiated by dropping 0.5 ml of the SWCNT solution sample into the separation column from the top, followed by adding successive 1.5 ml of 1% SDS solution after which movement of the SWCNT in the column was observed. A fraction of the SWCNTs were trapped at the top layer of the agarose beads, creating the “top band”, and another fraction of the SWCNT moved down through the column and eluted from the column as more 1% SDS solution was added, creating the “bottom band”. The eluted bottom band solution was collected. To elute the top band, 1% sodium deoxycholate (DOC, Sigma-Aldrich) in DIW was poured into the column, releasing it to the bottom and was collected. Generally, the top band corresponds to the semiconducting SWCNTs enriched sample (s-SWCNT), and the bottom band corresponds to the metallic SWCNT enriched (m-SWCNT) sample [10]. Fig. 1 shows the top and bottom band fractions during separation (Fig. 1a) and the corresponding m-SWCNT and s-SWCNT enriched fractions collected after separation (Fig. 1b) for CoMoCAT sample shown as example. The observable coloration of the separated samples are evident of succesful electronic type separation [11].

2.2 Resonance Raman Spectroscopy (RRS)

Optical characterization was done via RRS to estimate the tube defect level. The SWCNT samples before and after separation process were deposited on a Si wafer substrate with thermally grown SiO_2 surface layer via drop cast method and baked on a hot plate at 120 $^\circ\text{C}$ for 20 min or until completely dried. The substrates were then subjected to RRS measurement with 514 nm laser source in a commercial Renishaw microRaman spectrometer. The environment of the measurements was controlled at 24 $^\circ\text{C}$ under atmosphere conditions. The laser spot size was approximately 5 μm in diameter using sample objective lens of 50 times magnification (50X). To minimize noise signal originating from photo-response of the substrate and the SWCNTs, the measurements were done in a dark chamber. For every sample, the measurements were repeated three times at different spots or areas, therefore producing several Raman spectra. This was done to ensure reproducible and correct measurements. From the spectra of the measurements, the *G* and *D* peaks were noted and the *G/D* peak height ratios were calculated. The *G/D* peak height ratio is a marker for SWCNT structural tube defect level whereby a high value indicates structurally pure SWCNTs, whereas a low value corresponds to a high degree of structural defects [12].

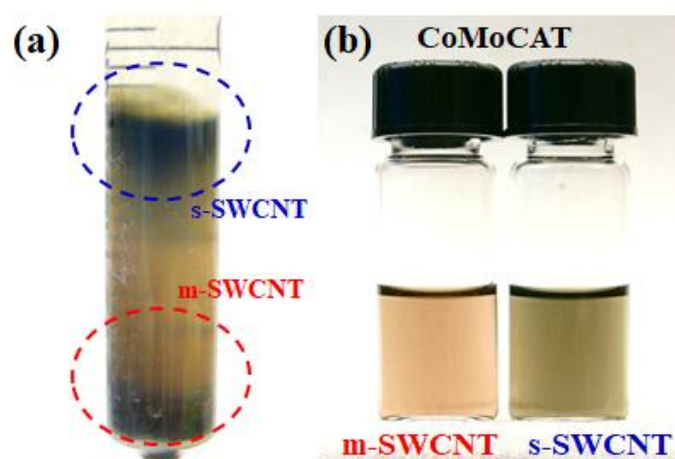


Fig. 1 – (a) A continuous separation syringe column with the formation of “top” and “bottom” bands, corresponding to s-SWCNTs and m-SWCNTs, respectively; (b) The collected separated SWCNTs samples based on electronic type. The s-SWCNT samples were used for CNTFET fabrication.

2.3 CNTFET Device Fabrication

The CNTFETs fabricated were based on a bottom contacted electrodes and substrate backgated structure on Si-SiO₂ substrate as shown in Fig. 2a. The s-SWCNT samples were deposited via spin coating on an n-type Si wafer with 250 nm SiO₂ top layer acting as the gate dielectric layer grown thermally. Au electrodes were patterned via photolithography prior to the s-SWCNT deposition and the doped substrate was contacted for the back-gate. Fig. 2b shows the scanning electron micrograph (SEM) of the device from the top view showing the s-SWCNT active channel contacting between source and drain electrodes. From the SEM analysis, the deposition of SWCNTs was controlled to have only a single tube or bundle connecting between the two electrodes. Details of the fabrication process was described previously in [11].

2.4 Electrical Characterization

Electrical characterization consisted of 3-terminal transistor measurements to produce the *I-V*, output and transfer characteristics of field effect transistor. The analyzer used was an industry standard Keithley 4200-SCS. From the measurements, key CNTFET device parameters were determined including the on-off current ratio, I_{ON}/I_{OFF} , transconductance, g_m , subthreshold slope, S_n , and field effect mobility, μ_{FE} , calculated based on reference [11].

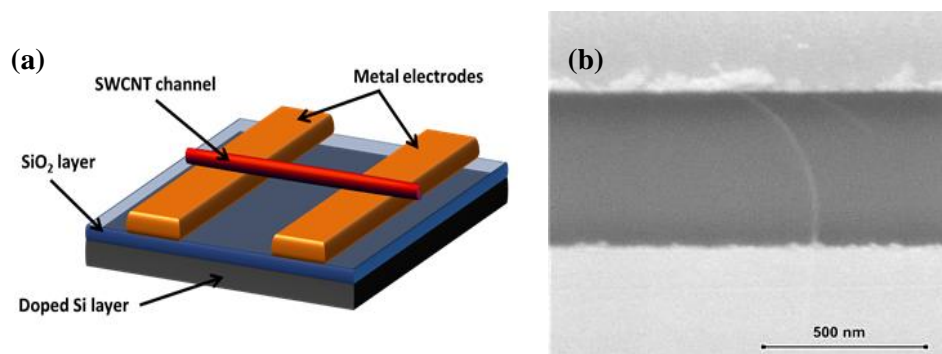


Fig. 2 – (a) An illustration of the CNTFET device structure consisting of a bottom contacted SWCNT active channel on pre-patterned Au electrodes on n-type doped Si wafer with thermally grown SiO₂; (b) The SEM micrograph of the top view of the device showing a single s-SWCNT as an active channel connecting the source and drain of the CNTFET.

3. Results and Analysis

The results and analysis section is divided into three subsections. The first part presents and discusses the optical characterization of SWCNT samples based on the RRS analysis. In the second part, we present and discuss the device measurements and electrical characterizations. The third part involves an analysis of the correlation between SWCNT defect level (the synthesis method of the source) and the CNTFET performance.

3.1 Resonance Raman Spectroscopy Results

From the Raman measurements of all samples, the Raman spectra of intensity versus Raman shift were plotted. Fig. 3 shows the Raman spectra about the radial breathing mode (RBM) peaks' range at Raman shifts around 100 – 350 cm⁻¹. The following Fig. 4 shows the Raman spectra within the *D* and *G* peaks' Raman shift range i.e. between 1200 to 1800 cm⁻¹. It should be noted that the Raman spectra in Fig. 3 and Fig. 4 have been normalized about the *G*⁺ peak height or intensity, which is a crucial step to ensure that direct intensity comparison between the spectra can be made correctly [11].

From Fig. 3, the RBM peaks are clearly observable for all SWCNT samples, confirming that the sample indeed consist of SWCNTs, as opposed to any other type of graphitic materials, including multi walled CNT (MWCNT). Other than that, the RBM peaks can also be used to estimate the tube diameter of the SWCNTs based on the relation $\omega_{RBM} = A/d_t + B$, where ω_{RBM} is the Raman shift of the RBM peak position, and the *A* and *B* parameters are determined empirically [12]. Preliminary analysis of the RBM peaks confirm the tube diameter distribution of all SWCNT samples as shown in Table 1.

The estimation of the SWCNT structural defect level can be estimated from the data shown in Fig. 4. The *G* and *D* peaks' heights, which are the intensity, were measured and the respective *G/D* ratios were calculated as shown as insets in Fig. 4. The calculated *G/D* ratios are also shown in Table 2.

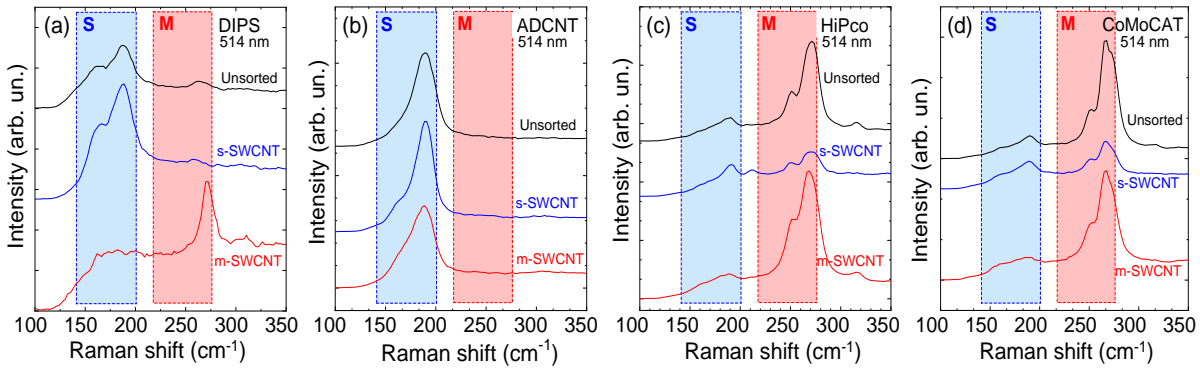


Fig. 3 – Raman spectra using 514 nm laser of all samples before and after separation process at the RBM Raman shift range for: (a) DIPSS; (b) ADCNT; (c) HiPco; (d) CoMoCAT. The black, blue and red spectra are the unsorted, s-SWCNT and m-SWCNT fractions, respectively. The blue and red shaded rectangle box indicate the Raman shift regions where the RBM peaks correspond to s-SWCNT and m-SWCNT, respectively.

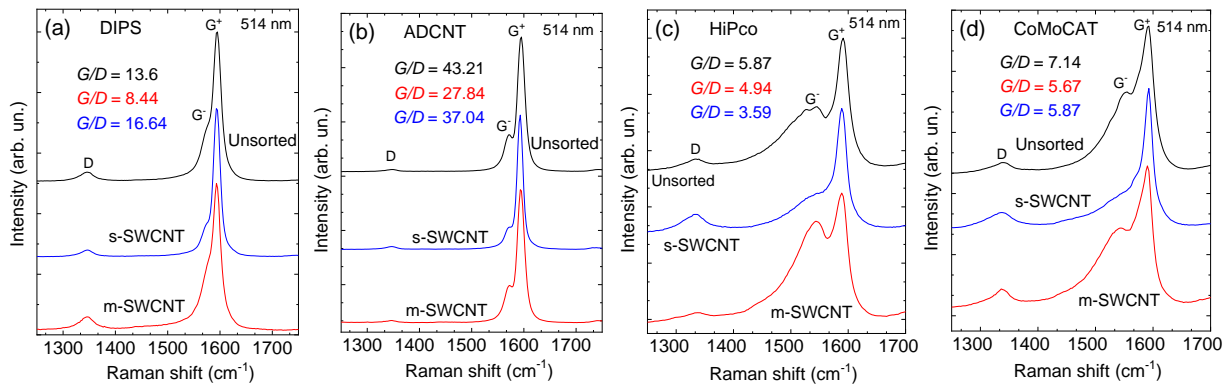


Fig. 4 – Raman spectra using 514 nm laser of all samples before and after separation process at the D and G peaks Raman shift range for: (a) DIPSS; (b) ADCNT; (c) HiPco; (d) CoMoCAT. The inset are the calculated G/D ratios for all spectra.

As shown in Fig. 4, the Raman spectra of all SWCNT samples before electronic type separation (Unsorted) and after separation i.e s-SWCNT and m-SWCNT are shown as black, blue and red spectra, respectively. It can be observed that the D/G ratios varies between samples, and are also different before and after the separation process. For the s-SWCNT samples that were used as the active channel of CNTFETs, the ADCNT sample displays the highest G/D , followed by DIPSS, CoMoCAT and HiPco in decreasing order. Similar decreasing order of variation of G/D is also observable to the samples before electronic type separation i.e unsorted samples. Therefore, based on the Raman analysis, in the order of decreasing defect level, sample HiPco has the highest defect level, followed by CoMoCAT, DIPSS and ADCNT. This also shows that sample ADCNT has the highest quality SWCNTs in terms of tube structure defect level, and sample HiPco displays the lowest quality SWCNTs.

3.2 Terminal Field Effect I - V Measurement

The electrical characterization of the CNTFETs consist of 3-terminal field effect I - V measurements that were carried out within controlled ambient environment. A total of 16 devices were measured, consisting of 4 devices from each s-SWCNT sample. The field effect transistor transfer characteristics of one device from each s-SWCNT sample as the active channel are shown in Fig. 5 on the same axes.

It can be observed from Fig. 5 that the transfer characteristics and hence the switching behavior display variation and correlation across the different source of s-SWCNT active channel. In general, every device demonstrated primarily p -type transistor behavior except for the DIPSS CNTFET where it instead showed strong ambipolar behavior that skews towards p -type. It can also be observed that the ADCNT CNTFET shows slight ambipolar behavior, evident by the two order of magnitude I_{DS} increase for V_{GS} between 20 to 30 volts. For HiPco and CoMoCAT CNTFETs, the transfer characteristics are very similar with HiPco displaying higher I_{ON} and I_{OFF} . The similar switching behavior is expected since both devices are based on SWCNTs of similar diameter distribution. The significant variation in the I_{ON} and I_{OFF}

currents therefore could be due to varying tube defect level. However, this is one possibility and inconclusive since channel with multiple SWCNTs may also result in increased or decreased drain current.

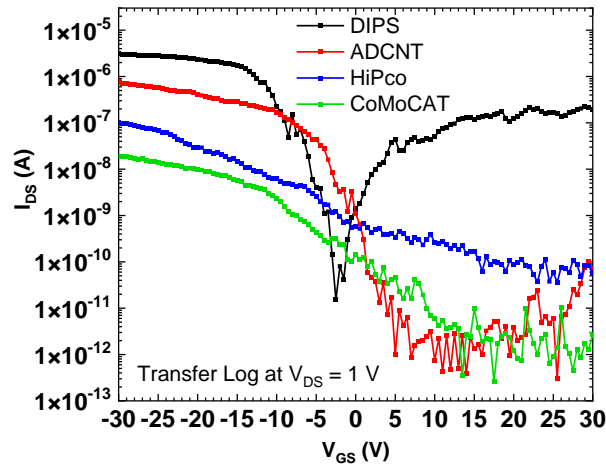


Fig. 5 – The 3-Terminal transfer characteristics of CNTFETs with different s-SWCNT active channel at drain-source voltage, $V_{DS} = 1$ V. The black, red, blue and green curves are the transfer characteristics of DIPS, ADCNT, HiPco and CoMoCAT devices, respectively.

Table 2 shows the average device parameters with respect to devices of different SWCNT channel source and G/D ratios. Here, observations to the key device parameters can be made as follows.

Firstly, the I_{ON} and I_{OFF} are different for each device type, yielding varying I_{ON}/I_{OFF} ratios. The I_{ON} was measured at $V_{GS} = -30$ V and the I_{OFF} were the minimum current values for each device. The average I_{ON} is the highest for DIPS, followed by ADCNT, HiPco and CoMoCAT, in decreasing order. Devices with HiPco and CoMoCAT have similarly low I_{ON} as expected due to the low G/D values. Devices with DIPS displayed an order of magnitude higher I_{ON} compared to ADCNT devices despite having much less G/D value. This can be attributed to the DIPS samples containing SWCNTs of larger diameters, hence lower bandgap. Therefore, although device conductivity can be affected by the SWCNTs' defect level, the diameter or bandgap effect dominates. The average I_{OFF} variation on the other hand correlates with the SWCNTs' defect level i.e. lower G/D display higher I_{OFF} . For DIPS devices, the I_{OFF} is still relatively higher, but this might be due to the ambipolar behavior where the threshold voltage of each mode overlaps. Consequently, the I_{ON}/I_{OFF} is therefore inversely proportional to the tube defect level whereby the correlation is true for all SWCNT samples.

Secondly, the correlation between the S_p , g_m and μ_{FE} to the SWCNT tube defect level can be observed from Table 2. The S_p generally increases as the tube defect increases i.e. decreasing G/D . Devices with DIPS show relatively lower S_p compared to ADCNT devices, which might be attributed to the tube capacitance effect of large diameter SWCNTs [5], [13]. For the g_m , the value generally decreases as the tube defect increases. Similarly, exception is for DIPS devices with higher g_m compared to that of ADCNT despite displaying lower G/D value since S_p is related to g_m . For the μ_{FE} parameter, it is clearly observed that it is directly proportional to the tube defect level whereby μ_{FE} increases as G/D increases. DIPS devices are second to ADCNT devices in terms of μ_{FE} despite displaying the highest g_m , which can be attributed to the former's relatively broader tube diameter distribution.

Table 2 – Key device parameters of CNTFETs with different SWCNT active channel source

Parameter (SWCNT Source)	ADCNT	DIPS	CoMoCAT	HiPco
	$G/D = 37.04$	$G/D = 16.64$	$G/D = 5.87$	$G/D = 3.59$
Average I_{ON} , (A)	3.29×10^{-7}	1.62×10^{-6}	1.27×10^{-7}	1.28×10^{-7}
Average I_{OFF} , (A)	2.61×10^{-12}	5.83×10^{-11}	9.48×10^{-11}	8.66×10^{-11}
Average I_{ON}/I_{OFF}	4.52×10^5	7.78×10^4	2.28×10^4	4.55×10^3
Average S_p , (mV/Dec)	1331	1168	8648	10000
Average g_m , (mS)	2.35×10^{-5}	2.17×10^{-4}	1.04×10^{-5}	1.08×10^{-5}
Average μ_{FE} , ($\text{cm}^2 \text{V}^{-1} \text{s}^{-1}$)	26.42	3.06	1.44	1.43

3.3 Correlation Analysis and Discussion

From the results shown, correlation between CNTFET performance to the SWCNT source can be analyzed. Based on the RSS results, different SWCNT sources of different growth methods exhibit varying intrinsic structural defect level i.e. G/D values. Whilst it is shown that the G/D does not affect the I_{ON} significantly, it does however affect the I_{OFF} at a higher degree, yielding I_{ON}/I_{OFF} that is directly proportional to G/D . The switching performance indicated by S_p and g_m shows consistent correlation to the G/D i.e. higher G/D correlates to higher switching performance.

Quantitatively, the varying degree of G/D i.e. tube defect or growth method, resulted in a proportional variation in the degree of device performance. Here, μ_{FE} is taken as the figure of merit. For example, DIPS exhibit ~54% less G/D value to that of ADCNT, whilst the latter displayed μ_{FE} of ~860% higher. Comparing between ADCNT and HiPco, the former has more than an order of magnitude higher G/D , and 20 times higher μ_{FE} .

4. Conclusion

CNTFETs were fabricated using four SWCNT samples of different growth methods, each exhibiting varying tube defect level from the RRS. The electrical measurement results show significant correlation to the tube defect level and therefore it can be concluded that SWCNT growth method can influence CNTFET device performance significantly. It is also shown that although SWCNTs from different synthesis process may result in CNTFETs with similar switching behavior, provided that the tube diameter is similar, the difference in tube defect level can affect the drain current.

Acknowledgement

The authors would like to thank the Government of Malaysia and the Ministry of Higher Education for providing the research funding used in this work under research grant FRGS/1/2021/TK0/UKM/02/29. The authors would also like to thank the University of Surrey and Universiti Kebangsaan Malaysia (UKM) for providing the research facility for data obtained in this work.

References

- [1] Jorio, A., Dresselhaus, G., Dresselhaus, M. S., (2008). Carbon nanotubes: Advanced topics in synthesis, structure properties and applications, Berlin: Springer-Verlag.
- [2] Collins, P., Arnold, M., and Avouris, P., (2001). Engineering carbon nanotubes and nanotube circuits using electrical breakdown. *Science*, vol. 292, no. 5517, 706-709.
- [3] He, M. S., Zhang, S. C., Zhang, J., (2020). Horizontal Single-Walled Carbon Nanotube Arrays: Controlled Synthesis, Characterizations, and Applications, *Chemical Reviews*, vol. 120, no. 22, 12592-12684.
- [4] Tseng, Y-C., Phoa, K., Carlton, D., and Bokor, J., (2006). Effect of diameter variation in a large set of carbon nanotube transistors. *Nano Letters*, vol. 6, no.7, 1364-1368.
- [5] Zhang, Y. M., Yang, Y., Yang, T., et al, (2021). A Compact Physical Drain Current Model of Multitube Carbon Nanotube Field Effect Transistor Including Diameter Dispersion Effects. *IEEE Transactions on Electron Devices*, vol. 68, no. 12, 6571-6579.
- [6] Kastner, M., Stahl, S., Vollert, I., Loi, C., Ruhl, N., Hertel, T., et al, (2015). A comparison of Raman and photoluminescence spectra for the assessment of single-wall carbon nanotube sample quality. *Chemical Physics Letters*, 635, 245-249.
- [7] Saito, T., Xu, W., Ohshima, S., et al., (2006). Supramolecular catalysts for the gas-phase synthesis of single-walled carbon nanotubes, *Journal of Physical Chemistry B*, vol. 110, no. 12, 5849-5853.
- [8] Nikolaev, P., Bronikowski, M. J., Bradley, R. K., et al., (1999). Gas-phase catalytic growth of single-walled carbon nanotubes from carbon monoxide, *Chemical Physics Letters*, vol. 313, no. 1-2, 91-97.
- [9] Alvarez, W. E., Kitiyanan, B., Borgna, A., (2001). Synergism of Co and Mo in the catalytic production of single-wall carbon nanotubes by decomposition of CO, *Carbon*, vol. 39, no. 4, 547-558.
- [10] Tanaka, T., Urabe, Y., Nishide, D., et al., (2009). Continuous Separation of Metallic and Semiconducting Carbon Nanotubes Using Agarose Gel, *Applied Physics Express*, vol. 2, no. 12.
- [11] Yahya, I., Bonaccorso, F., Clowes, S. K., Ferrari, A. C., Silva, S. R. P., (2015). Temperature dependent separation of metallic and semiconducting carbon nanotubes using gel agarose chromatography, *Carbon*, vol. 93, pp. 574-594.
- [12] Dresselhaus, M., Dresselhaus, G., Saito, R., et al., (2008). Raman spectroscopy of carbon nanotubes, *Physics Reports-Review Section of Physics Letters*, vol. 409, no. 2, 47-99.
- [13] Khademhosseini, V., Dideban, D., Ahmadi, M. T., et al, (2019). The impact of vacancy defects on the performance of a single-electron transistor with a carbon nanotube island. *Journal of Computational Electronics*, vol. 18, no. 2, 428-435.